Design and simulation of asymmetric Y-junction beam splitter with controllable splitting based on adjusted air-hole defect

Phachara Phongwisit, Surachart Kamoldilok, Prathan Buranasiri, Keerayoot Srinuanjan* and Pichet Limsuwan

Department of Physics, School of Science, King Mongkut's Institute of Technology Ladkrabang, Bangkok 10520, Thailand. *e-mail: keerayoot.sr@kmitl.ac.th

Received: 19.05.2022

Abstract. We report a construction of a new asymmetric Y-junction beam splitter with a controllable splitting ratio and simulate this splitter. The splitter is based on InP, has the area 65.0 μm^2 and operates at the light wavelengths 1.48 and 1.55 μm. Under condition of no air-hole defect, the splitting ratio for the output ports 1 and 2 is equal to 92/8 at the both wavelengths. To control the splitting ratio, air-hole defects with different (diamond, square and cylinder) shapes are introduced at the junction between the two output ports. Our simulations confirm that the splitting ratio of the beam splitter can be efficiently controlled by changing the size and the shape of the air-hole defect. The maximal splitting ratios at our operating wavelengths are equal to 10/90 and 14/86 and the appropriate average insertion losses amount to 0.36 and 0.31 dB for all of defect shapes.

Keywords: adjustable beam splitters, waveguides, Y-junctions, integrated photonics

UDC: 621.39

1. Introduction

Optical waveguides represent useful photonic-crystal structures applied in different photonic and integrated-circuit (PIC) devices. These structures are designed to confine and guide propagation of electromagnetic waves of either visible or invisible ranges in optical communication networks. Confining and guiding phenomena in optical waveguides depend on the contrast of refractive indices of core (n_{core}) and cladding (n_{clad}), which provide the conditions of total internal reflection [1, 2].

Beam-splitting (or power-splitting) optical waveguides are basic components that split or separate optical waves from an input to two or more outputs. These devices are usually based on the well-known multimode interference (MMI) or Y-junction (Y-branch) structures. Optical splitting in the MMI splitters is associated with a self-imaging effect. This structure provides a large number of output ports with equal intensities at each of them and a highly uniform splitting. However, the MMI splitters are normally designed for operating in a narrow wavelength region [3–6]. On the other hand, the Y-junction splitters are aimed to split the light within broadband wavelength regions, while their splitting ratio can be adjusted either to be uniform or equal to some specific value by choosing the structure of the Y-junction.

Symmetric Y-junctions based on S-bend waveguides are very interesting for developing 1×2 or 1×N beam splitters. Nonetheless, the symmetric Y-junction structures must have relatively large areas of square millimetre scales in order to separate optical beams with highly uniform outputs [7–9]. An alternative method for developing 1×2 beam splitters with different splitting ratios is based upon asymmetric Y-junctions. A difference in geometric parameters and brunching angles in an output waveguide can provide non-uniform splitting with different splitting ratios basing on the PIC platform [10–12].

* Corresponding author

In the present work, we present a beam splitter designed on the asymmetric Y-junction waveguide, which reveals an important feature of controllable (including non-uniform) splitting ratio. Our beam splitter is based on InP and operates at the light wavelengths 1.48 and 1.55 μm. The air-hole defect at the Y-junction can be set to have different sizes and shapes. Simulations performed using finite-difference time-domain software have demonstrated different adjustable splitting ratios, in particular non-uniform and uniform outputs. The operating wavelengths of 1.48 and 1.55 μm are chosen in order to work with standard erbium-doped fibre-amplifier systems.

2. Modelling and simulation

To operate the beam splitter in uniform and non-uniform regimes at the both operating wavelengths, we chosen the substrate area of about 65.0 μm^2. Our beam-splitting waveguide was built on indium phosphide (the refractive index $n_{core} = 3.16$), with the refractive indices of substrate and cladding being equal to $n_{clad} = n_{substrate} = 1$. Fig. 1 shows a schematic design of our asymmetric Y-junction waveguide. Its dimensions (width×thickness×length) were 1×1×13 μm^3 and the branching angle between the output ports 1 and 2 amounted to 45°. An air-hole defect with the refractive index $n_{defect} = 1$ was introduced into the junction between the output ports. Then we measured the optical transmission of the both ports. We compared the air-hole defects with three different shapes (diamond, square and cylinder). The size of the diamond-shaped defect was defined as the distance between the opposite tips, the size of the square-shaped defect as the width of the square, and the size of the cylinder-shaped defect as the diameter of the cylinder. The sizes of the air-hole defects were studied in the region from 0.20 to 0.50 μm, with the increasing step of 0.01 μm. To measure the ratios of splitting between the output ports 1 and 2, light waves with the wavelengths 1.48 and 1.55 μm corresponding to transverse electric TE mode were launched into the waveguide.

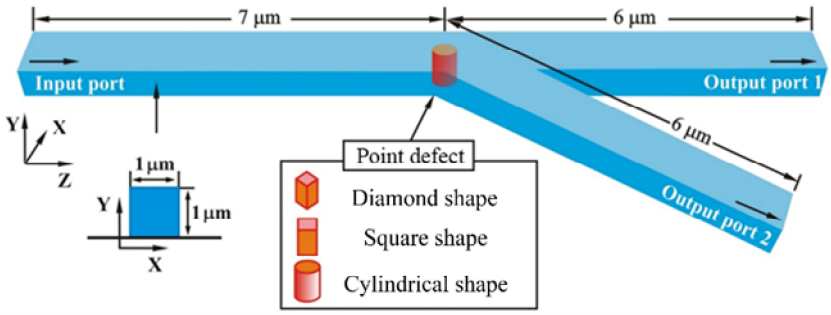

Fig. 1. Schematic design of our asymmetric Y-junction waveguide.

The beam splitter was simulated with a standard finite-difference time-domain method [13], using commercial software OptiFDTD. To study the influence of the air-hole defect on the asymmetric Y-junction, we compared the optical transmissions at the output ports 1 and 2. The splitting ratio was found from the relation [14]

$$\%T_n = (P_{On} / (P_{O1} + P_{O2})) \times 100\%, \quad (1)$$

where $\%T_n$ is the optical transmission calculated at the output ports 1 or 2, and P_{O1} and P_{O2} are the output intensities at the ports 1 and 2, respectively.

The insertion loss (IL), an important parameter characterizing performance of an optical component, was defined as the ratio of the normalized input power (P_{in}) to the total transmission power at the both output ports (in decibels, dB):

$$\mathrm{IL} = 10 \log(P_{in} / (P_{O1} + P_{O2})). \quad (2)$$

3. Results

In this section we report and discuss the results concerned with the simulated optical transmissions at the output ports, and the corresponding splitting ratio. Fig. 2 shows the electric-field propagation inside the waveguide with no air-hole defect. The optical transmission at the output port 1 is equal to 92% and that at the port 2 to 8% at the both wavelengths 1.48 and 1.55 μm. Fig. 2 illustrates also the electric-field distribution inside the waveguide at the input and output ports.

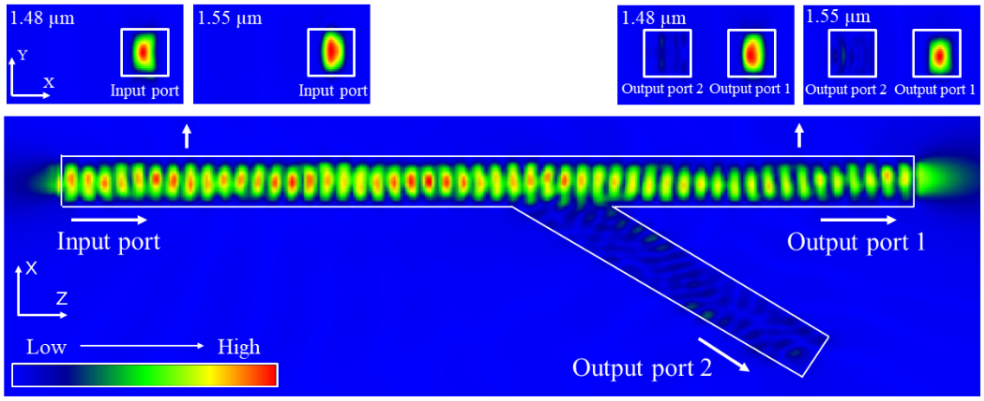

Fig. 2. Electric-field propagation at the input and output ports of our asymmetric Y-junction waveguide having no point defect (the operating wavelengths 1.48 and 1.55 μm). The frames of the waveguide are in white, blue colour corresponds to low intensities of the TE wave and red to high intensities.

3.1. The operating wavelength 1.48 μm

Below we present the simulation results obtained for the three shapes of defects at the wavelength of 1.48 μm. Fig. 3 shows the dependences of optical transmission on the defect size, where black and red lines refer respectively to the output ports 1 and 2.

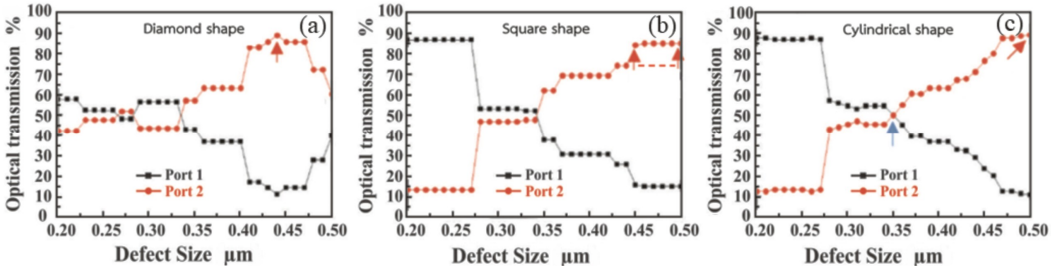

Fig. 3. Dependences of optical transmission on the defect size, as simulated for the asymmetric Y-junction waveguides with the air-hole defects (operating wavelength 1.48 μm): panels (a), (b) and (c) correspond respectively to diamond, square and cylindrical shapes of the defect.

At the smallest size of diamond-shaped defect, the optical transmissions at the output ports 1 and 2 are equal respectively to 58% and 42% (see Fig. 3a). With increasing defect size, the optical transmission decreases at the port 1 and increases at the port 2. On the other hand, the optical transmission at the output port 2 increases in the region 0.33–0.44 μm of defect sizes and reaches its maximum, 88%, at the size 0.44 μm (see the red arrow in Fig. 3a).

The optical transmission at the output ports 1 and 2 amounts respectively to 87% and 13% at the smallest size of square-shaped defect (see Fig. 3b). When the defect size increases, the optical transmission decreases at the port 1 and increases at the port 2. In the defect-size region 0.27–0.46 μm, the optical transmission at the output port 2 increases. It acquires the maximum of 85% at the sizes 0.46–0.50 μm (see the area between red arrows in Fig. 3b).

The optical transmissions at the ports 1 and 2 are equal respectively to 87.5% and 12.5% at the smallest size of defect of cylindrical shape (see Fig. 3c). Then the optical transmission at the port 1 (port 2) decrease (increases) with increasing defect size. Finally, the transmission at the output port 2 increases in the defect-size region 0.26–0.50 μm and achieves its maximal value 90% at the size 0.50 μm, as shown by red arrow in Fig. 3b.

3.2. The operating wavelength 1.55 μm

Now we report the simulation results obtained for the three shapes of defects at the wavelength 1.55 μm. Fig. 4 shows the dependences of optical transmission on the defect size, as calculated for the output ports 1 (black line) and 2 (red line).

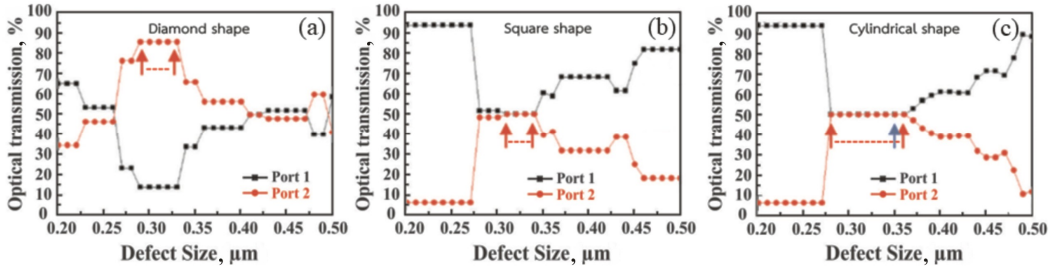

Fig. 4. Dependences of optical transmission on the defect size, as simulated for the asymmetric Y-junction waveguides with the air-hole defects (operating wavelength 1.55 μm): panels (a), (b) and (c) correspond respectively to diamond, square and cylindrical shapes of the defect.

As seen from Fig. 4a, the optical transmission is 65% at the output port 1 and 34% at the output port 2 at the smallest size of diamond-shaped defect. In the region 0.20–0.33 μm, increasing defect size causes decreases in the optical transmission at the output port 1 and its increase at the output port 2. At the other defect sizes, the transmission increases at the port 1 and decreases at the port 2. The maximal transmission at the port 2 is equal to 86% in the defect-size region 0.29–0.33 μm (see the area between red arrows in Fig. 4a).

As seen from Fig. 4b, the optical transmissions at the ports 1 and 2 are equal respectively to 94% and 6% at the smallest size of square-shaped defect. When the defect size increases in the region 0.20–0.34 μm, the transmission decreases at the port 1 and increases at the port 2. At the other sizes, the optical transmission increases at the port 1 and decreases at the port 2. The maximal optical transmission at the output port 2 (50%) can be reached at the defect sizes 0.31–0.34 μm (see the area between red arrows in Fig. 4b).

The optical transmission at the output ports 1 and 2 amount respectively to 94% and 6% at the smallest size of cylindrical defect (see Fig. 4c). When the defect size increases in the region 0.20–0.36 μm, the optical transmission decreases at the port 1 and increases at the port 2. However, the transmission increases at the port 1 and decreases and the port 2 at the other sizes. The maximum at the port 2 (50%) corresponds to the defect sizes 0.28–0.36 μm (see the area limited by red arrows in Fig. 4c).

3.3. Field distribution and IL

Fig. 5 shows the field distribution in the X-Z plane simulated for the asymmetric Y-junction beam-splitting waveguide with the 0.35-μm cylindrically shaped defect. Here the field distributions at the both operating wavelengths correspond to the uniform splitting at the points indicated by blue arrows in Fig. 3c and Fig. 4c. The ILs for this uniform beam splitter are equal to 0.28 and 0.46 dB at the wavelengths 1.48 and 1.55 μm, respectively.

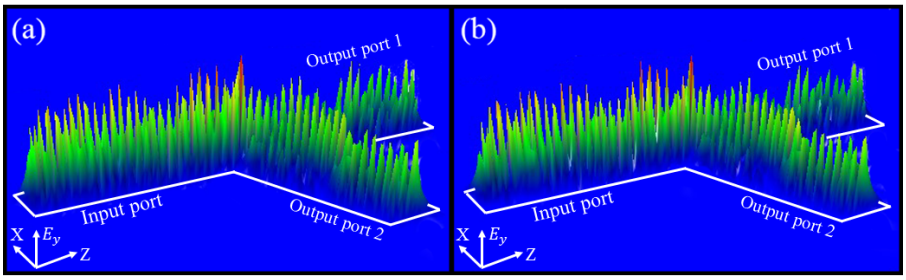

Fig. 5. Field distributions inside the asymmetric Y-junction beam-splitting waveguide with the 0.35-μm cylindrically shaped defect: panels (a) and (b) correspond to the uniform output achieved respectively at the operating wavelengths 1.48 and 1.55 μm.

The IL values calculated for the asymmetric Y-junction waveguide with no defect are 0.05 and 0.09 dB for the two operating wavelengths. After the defect is introduced, the average IL increases at the both operating wavelengths. The average IL values calculated for the beam splitters with diamond-, square- and cylinder-shaped defects operating at 1.48 μm are 0.42, 0.33 and 0.32 dB, respectively. The same parameters calculated at 1.55 μm are equal respectively to 0.31, 0.20, and 0.41 dB.

4. Discussion

By comparing the optical transmissions at the output ports 1 and 2 (see data of Fig. 3 and Fig. 4), one can find the corresponding splitting ratios of our splitter. In particular, Table 1 shows some optical ratios useful for different PIC applications (20/80, 25/75, 30/70, 33/67, 40/60, 50/50, 60/40, and 75/25).

Table 1. Splitting ratios corresponding to different defect shapes and operating wavelengths.

Defect shape	Splitting ratio	
	Operating wavelength 1.48 μm	Operating wavelength 1.55 μm
Diamond	15/85	33/66, 40/60, 50/50
Square	15/85, 25/75, 30/70	50/50, 60/40, 75/25
Cylinder	10/90, 20/80, 33/67, 40/60, 50/50	50/50, 60/40

At the operating wavelength 1.48 μm, the diamond-shaped defect with the size 0.43 μm implies the splitting ratio 15/85. The square-shaped defects with the sizes 0.46–0.50, 0.43–0.44 and 0.37–0.42 μm yield in the splitting ratios 15/85, 25/75 and 30/70, respectively. Finally, the cylindrically shaped defects with the sizes 0.50, 0.46, 0.42, 0.38 and 0.35 μm correspond to the splitting ratios 10/90, 20/80, 33/67, 40/60 and 50/50, respectively.

Concerning the operating wavelength 1.55 μm, the diamond-shaped defects with the sizes 0.34–0.35, 0.48–0.49 and 0.41–0.42 μm produce respectively the splitting ratios 33/66, 40/60, and 50/50. The square-shaped defects with the sizes 0.31–0.34, 0.35 and 0.45 μm correspond to the splitting ratios 50/50, 60/40 and 75/25, respectively. Finally, the cylindrically shaped defects with the sizes 0.25–0.35 and 0.42–0.43 μm provide the splitting ratios 50/50 and 60/40, respectively.

As seen from Table 1, control of the size of cylindrically shaped defects can result in both uniform and non-uniform splitting at the two operating wavelengths, involving various sufficiently different values of the splitting ratio. This implies that the beam splitters with the cylinder-shaped defects represent the devices which are the most suitable for various optical PIC components.

In Table 2 we compare the main parameters of our 1×2 beam splitter with those of the common 1×2, 1×4 and 1×N beam splitters, which are based on different structure types. The beam

splitters known from the literature (see Refs. [4, 7, 10, 15–17]) are designed on MMI-based, two-folded and Y-junction waveguides. Typically they require large enough areas (more than 1 mm^2) to separate the optical waves at the uniform outputs. On the other hand, the technical solution [18] requires the operating area of only ~ 60.7 μm^2. This is similar to our beam splitter, although the specific splitting mechanism [18] is associated with the photonic bandgap, which can complicate the PIC fabrication process.

It is important that the non-uniform splitting regime of our beam splitter is easily achievable by a choice of size and shape of the air-hole defect (see Table1). This feature is similar to that of the splitters reported in Refs. [11, 19]. In particular, the splitting ratio in Ref. [11] can be governed by relocating a triangular air hole with the size 2 μm. There the process of relocation of the air hole in the range 0.25 μm away from the waveguide junction provides different splitting ratios at the two output ports, with the average IL ~ 0.49 dB. On the other hand, the splitting ratio in Ref. [19] is controlled by adjusting the size of a nanoscaled air hole at a T-branch of beam-splitter junction, with the IL being about 0.92 dB.

Table 2. Comparison of different beam splitters known from the literature.

Reference	Type of structure	Operating wavelength, μm	Splitting ratio	Size of device, μm^2	IL, dB
This work	1×2 asymmetric Y-junction	1.48/1.55	20/80, 25/75, 30/70, 33/67, 40/60, 50/50, 60/40, 75/25	~ 65.0	~ 0.35 (1.48 μm) ~ 0.31 (1.55 μm)
[4]	1×N MMI waveguide	1.55	uniform	~ 8.3×10^3	~ 1.00 (1×6 beam splitter)
[7]	1×2 symmetric Y-junction	1.55	uniform	~ 1.4×10^6	~ 13.00
[10]	1×4 asymmetric Y-junction	1.55	uniform	~ 5.7×10^6	~ 0.08
[11]	1×2 photonic bandgap splitter with relocated triangular air hole	1.55	50/50, 60/40, 70/30, 80/20	~ 34.0	~ 0.49
[15]	1×10 MMI waveguide with 1×10 directional couplers	1.55	uniform	~ 28.7×10^3 ~ 1.76×10^5	~ 0.16 (MMI) ~ 0.54 (DC)
[16]	1×2 two-folded self-aligned pedestal waveguide	1.55	uniform	~ 33.0×10^3	~ 0.13
[17]	1×2 symmetric polymer-based Y-junction	1.55	uniform	~ 38.1×10^3	~ 3.56
[18]	1×2 Y-junction photonic-crystal waveguide	1.55	uniform	~ 60.7	0
[19]	1×2 T-branch waveguide mirrors	1.54–1.58	20/80, 30/70, 40/60	~ 49.0	~ 0.92

Returning to the result of this work, we remind that our device has a sufficiently small size (around 65.0 μm^2) and can provide a uniform splitting regime at the both operating wavelengths. After adjusting the defect sizes and shapes, a non-uniform splitting regime can be reached with a smaller IL (0.35 dB at 1.48 μm and 0.31 dB at 1.55 μm). Of course, the size of the beam-splitting device is of great importance for any PIC application. As a matter of fact, a smaller size gives a possibility to construct a larger number of beam splitters on a single integrated chip, which would provide different splitting ratios.

5. Conclusions

In the present work, we report a design of the beam splitter with controllable splitting ratio, which is based on the asymmetric Y-junction waveguide, and simulate the work of this splitter. Our beam splitter is made of InP and operates at the standard light wavelengths 1.48 and 1.55 μm. The dimensions of the beam splitter are 1×1×13 μm^3. The results of simulations performed with the finite-difference time-domain software reveal the relations between the size and shape of the air-hole defect, on the one hand, and the splitting ratio of the beam splitter, on the other hand.

Different splitting ratios that involve both uniform and non-uniform output regimes can be achieved with our device. At the specific sizes of diamond-shaped defects, the beam splitter can provide a useful splitting ratio 15/85 at the operating wavelength 1.48 μm and a number of ratios (e.g., 33/66, 40/60 and 50/50) at 1.55 μm. The beam splitter with the square-shaped defects can ensure the splitting ratios 25/75 and 30/70 at 1.48 μm and the ratios 50/50, 60/40 and 75/25 at 1.55 μm. Finally, different sizes of cylindrically shaped defects also correspond to a number of useful splitting ratios (10/90, 20/80, 33/67, 40/60 and 50/50 at 1.48 μm, and 50/50 and 60/40 at 1.55 μm).

We note that the beam splitter suggested in this work manifests a small enough size and can be applied for splitting optical beams under condition of controllable splitting ratios. This device is suitable for various optical communication systems built on PIC technologies.

Funding: This research has received no external funding.

Conflicts of interest: The authors declare no conflict of interest.

References

1. Pollock C and Lipson M. Integrated Photonics. Boston: Springer, 2003.
2. Boudrioua A. Photonic Waveguides: Theory and Applications. New York: John Wiley and Sons, 2009.
3. Blahut M and Kasprzak D, 2004. Multimode interference structure – properties and application. Opt. Applicata. **34**: 573–587.
4. Hosseini A, Kwong D N, Zhang Y, Subbaraman H, Xu X and Chen R T, 2011. 1×N multimode interference beam splitter design techniques for on-chip optical interconnections. IEEE J. Select. Top. Quant. Electron. **17**: 510–515.
5. Han L, Liang S, Zhu H, Zhang C and Wang W, 2015. A high extinction ratio polarization beam splitter with MMI couplers on InP substrate. IEEE Photon. Techn. Lett. **27**: 782–785.
6. Pan C and Rahman B M, 2016. Compact polarization-independent MMI-based 1×2 power splitter using metal-cap silicon-on-insulator waveguide. IEEE Photon. J. **8**: 3.
7. Singhal R, Satyanarayan M N and Pal S, 2012. Fabrication of single-mode Y-branch waveguides in photosensitive polymer with reduced Y-junction residue. Optik. **123**: 1911–1914.
8. Sun S M, Sun Y L, Zheng B Y, Wang P, Hou Z S, Dong W F, Zhang L, Chen Q D, Tong L M and Sun H B, 2016. Protein-based Y-junction optical micro-splitters with environment-

stimulus-actuated adjustment. Sens. Actuators B Chem. **232**: 571–576.
9. Ren Y, Zhang L, Xing H, Romero C, Vázquez de Aldana J R and Chen F, 2018. Cladding waveguide splitters fabricated by femtosecond laser inscription in Ti:sapphire crystal. Opt. Las. Technol. **103**: 82–88.
10. Tang X, Liao J, Li H, Zhang L, Lu R and Liu Y, 2010. A novel scheme for 1×N optical power splitter. Opt. Express. **18**: 21697–21704.
11. Yang L C, Huang C C, Huang H C and Tsao S L, 2012. A novel 1×2 optical power splitter with PBG structures on SOI substrate. Optik. **123**: 306–309.
12. Ab-Rahman M S, Aziz A N A, Nordin R and Jumari K, 2020. Optimum design of an optical waveguide: determination of the branching angle of s-bend waveguides. Optik. **200**: 163249.
13. Kawano K and Kitoh T. Introduction to Optical Waveguide Analysis. New York: John Wiley and Sons, 2001.
14. Wang H-T, Chen C-F, Chi S A, 2019. Numerical solution for broadband PLC splitter with variable splitting ratio based on asymmetric three waveguide structures. Appl. Sci. **9**: 1892.
15. Lunghi T, Doutre F, Rambu A P, Bellec M, De Micheli M P, Apetrei A M, Alibart O, Belabas N, Tascu S and Tanzilli S, 2018. Broadband integrated beam splitter using spatial adiabatic passage. Opt. Express. **26**: 27058–27063.
16. Roggero U F S and Hernández-Figueroa H E, 2020. Polymeric power splitters for multiplexing optical biosensors. Opt. Las. Technol. **127**: 106127.
17. Gašo P, Pudiš D, Seyringer D, Kuzma A, Gajdošová L, Mizera T and Goraus M, 2021. 3D polymer based 1×4 beam splitter. J. Lightwave Technol. **39**(1): 154–161.
18. Moumeni I and Labbani A, 2021. Very high efficient of 1×2, 1×4 and 1×8 Y beam splitters based on photonic crystal ring slot cavity. Opt. Quant. Electron. **53**: 129.
19. Zhong Z, Liu Y, Wang S, Liu Y, Jin H, Song Q and Xu K, 2021. T-branch waveguide mirror for multimode optical splitter with arbitrary power ratios. IEEE J. Quant. Electron. **57**: 6300306.

Phachara Phongwisit, Surachart Kamoldilok, Prathan Buranasiri, Keerayoot Srinuanjan and Pichet Limsuwan. 2022. Design and simulation of asymmetric Y-junction beam splitter with controllable splitting based on adjusted air-hole defect. Ukr.J.Phys.Opt. **23**: 142 – 149. doi: 10.3116/16091833/23/3/142/2022

Анотація. *Ми повідомляємо про нову конструкцію асиметричного подільника з Y-подібним переходом із регульованим коефіцієнтом розщеплення, а також моделюємо роботу цього подільника. Подільник побудований на InP, має площу 65,0 мкм^2 і працює на світлі з довжинами хвиль 1,48 і 1,55 мкм. За умови відсутності дефекту повітряного отвору коефіцієнт розщеплення для вихідних портів 1 і 2 дорівнює 92/8 на обох робочих довжинах хвилі. Для контролю коефіцієнта розщеплення на стику між двома вихідними портами вводять дефекти повітряних отворів різних (ромбічної, квадратної та циліндричної) форм. Моделювання підтверджує, що коефіцієнт розщеплення світлоподільника можна ефективно контролювати, змінюючи розмір і форму дефекту повітряного отвору. Максимальні коефіцієнти розщеплення на наших робочих довжинах хвиль дорівнюють 10/90 і 14/86, а відповідні середні внесені втрати становлять 0,36 і 0,31 дБ для всіх форм дефектів.*